

# Vertebrae in Compression: Mechanical Behavior of Arches and Centra in the Gray Smooth-Hound Shark (*Mustelus californicus*)

Marianne E. Porter\* and John H. Long Jr.

Department of Biology, Vassar College, Poughkeepsie, New York 12604

**ABSTRACT** In swimming sharks, vertebrae are subjected, in part, to compressive loads as axial muscles contract. We currently have no information about which vertebral elements, centra, arch cartilages, or both, actually bear compressive loads in cartilaginous vertebrae. To address this issue, the goal of this experiment was to determine the load-bearing ability of arch and centrum cartilages in compression, to determine the material properties of shark vertebrae, and to document fracture patterns in the centra with and without the arches. Intact vertebrae and vertebrae with the arch cartilages experimentally removed (centra alone) were subjected to compressive loading to failure at a single strain rate. The maximum compressive forces sustained by the vertebrae and the centra are statistically indistinguishable. Thus we conclude that under these testing conditions the arch does not bear appreciable loads. Independent evidence for this conclusion comes from the fact that vertebrae fail in compression at the centra, and not at the arches. Overall, the results of these mechanical tests suggest that the neural arches are not the primary load-bearing structure during axial compression. *J. Morphol.* 271:366–375, 2010. © 2009 Wiley-Liss, Inc.

**KEY WORDS:** axial skeleton; elasmobranch; material properties; mineralized cartilage

## INTRODUCTION

Vertebral centra, the mineralized skeletal segments that create joints along the notochord, have evolved independently at least four times, in elasmobranchs, actinopterygians, dipnoans, and tetrapods (Schaeffer, 1967; Laerm, 1979; Gardiner, 1983; Arratia et al., 2001). What adaptive value did centra provide? We propose that the evolution of vertebrae was driven, in part, by selection for enhanced swimming performance (Doorly et al., 2009). With the addition of centra to a notochord, the axial skeleton becomes stiffer in bending (Long et al., 2004). In addition, centra are hypothesized to stiffen the axial skeleton in compression (Clark, 1964; Laerm, 1976; Wainwright et al., 1978). Such structural stiffness of the axial skeleton is linearly proportional to steady swimming speed in robotic fish models (Long et al., 2006), and might be expected to have similar effects in animal lineages. Although from mechanical first principles it

appears obvious that adding stiff elements to a flexible notochord would stiffen the whole column, we must keep in mind that other skeletal elements, i.e., the neural and hemal arches (see Fig. 1), were already part of the vertebral column before centra evolved. To what extent was vertebral column stiffness increased by the addition of centra? Although we know that centra are able to handle large compressive loads (Porter et al., 2006, 2007), what remains untested is the mechanical behavior of vertebrae with and without arches.

For our study system, we chose sharks because (1) their centra and arches are not fused together, allowing easy dissection of the two structures, (2) their centra can be modeled as simple cylinders (Goodrich, 1930), simplifying interpretation of mechanical behavior, and (3) their arches are formed by a continuous series of skeletal elements that span the intervertebral joints, allowing for the possibility that they bear significant compressive loads over many body segments. In contrast, the vertebrae of bony fish are often structurally complex, with arch elements fused to centra, robust zygapophyseal articulations, and neural and hemal arches extended as spines (Long, 1992; Koob and Long, 2000). Bearing in mind the simpler vertebral anatomy of sharks, compressive loads can be borne by either the column formed by the serially arranged centra, the column formed by the serially arranged neural and interdorsal arch cartilages (= “arch cartilages”), or both columns in parallel.

Although vertebral strains have never been measured in sharks, their vertebrae are likely to experience compression under loads (see Fig. 2)

Contract grant sponsor: National Science Foundation; Contract grant numbers: IOB-0616322, DBI-0442269, IOS-0922605.

\*Correspondence to: M. E. Porter, Department of Biology, Vassar College, 124 Raymond Ave., Box 731, Poughkeepsie, New York 12604. E-mail: meporter@vassar.edu

Received 11 July 2009; Revised 25 August 2009; Accepted 25 August 2009

Published online 27 October 2009 in Wiley InterScience (www.interscience.wiley.com) DOI: 10.1002/jmor.10803

created by (1) contracting myomeric muscles whose line of action is oblique with respect to the axis (Donley and Shadwick, 2003; Donley et al., 2004; Gemballa et al., 2006) and (2) hydrodynamic forces acting on the body (Vogel, 1994). When muscles are active, compression loads the vertebrae as part of the axial bending of undulatory swimming (Wainwright et al., 1976; Vogel, 2003). In addition, pure compressive loads may be applied transiently during a fast start, if bilateral activation is present (Westneat et al., 1998; Hale

et al., 2002; Tytell and Lauder, 2002; Fig. 2A). Hydrodynamic loading occurs if the shark is moving, with compressive loads on the vertebrae applied by drag and thrust during swimming; pure compression may be present when the body is held straight, as in gliding, or locally as a bending joint passes through a straight posture (Fig. 2B).

In the experiments reported here, we had two goals. First, we compress the vertebrae (see Fig. 1) of smooth-hound sharks, *Mustelus californicus*, with and without the associated arches (see Fig. 3), measuring and comparing maximum force at failure (N), ultimate strength (MPa), yield strength (MPa), yield strain (%), and Young's modulus (MPa). The ideal experiment of independently measuring the properties of the arch, centrum, and vertebrae gave way to measuring the centrum and the arch-plus-centrum (denoted as the "centra" and "vertebrae" conditions, respectively) because the arches could not be tested without slipping. This ablation approach is inspired by measurements of bone material properties with and without trabeculae (Rogers and LaBarbera, 1993). Second, we compressed vertebrae and centra until they failed, observing and categorizing their fracture patterns. From our previous compression tests on centra only, we expected centra to fail by fracturing along annuli or by cracking radially (Porter et al., 2006). The presence of the arches may redistribute the load and cause different kinds or amounts of failure. Vertebral fractures may occur in living cartilaginous fishes, as suggested by multivertebrae pathologies that are apparent responses to trauma (Hoenig and Walsh, 1983; Heupel et al., 1999; Porter et al., 2006). Unfortunately, not enough is known about *in vivo* vertebral fractures to allow comparison with our *in vitro* patterns. Vertebral fractures, if they do

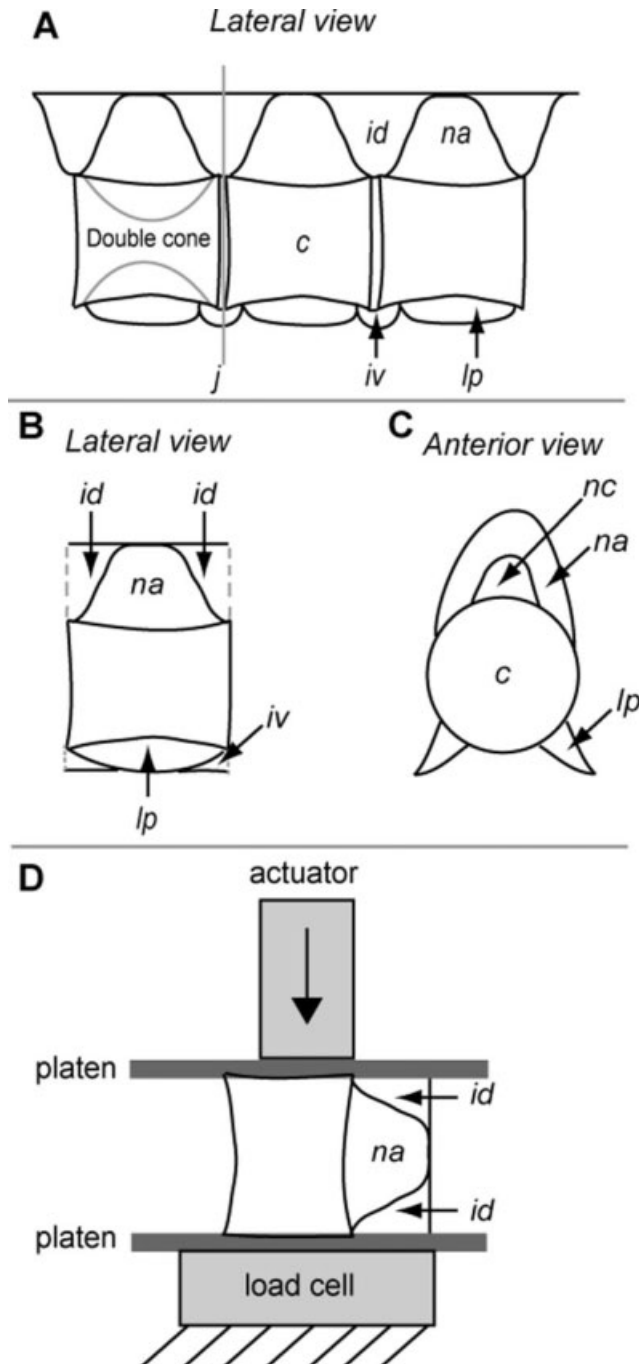


Fig. 1. Precaudal vertebrae and compression tests. **A:** Generalized anatomy of mineralized centra and arch cartilages, modified from Goodrich (1930). Arch cartilages located dorsal to the centra (c) include the neural arches (na) and the interdorsals (id), which form a continuous span (see transverse view in C, below). Lateral processes located ventral to the centra are homologous with hemal arches caudally (not figured). Mid-sagittal interior view in left-most centrum shows the double cone structure that forms two halves of amphicoelous joints (j) anteriorly and posteriorly. **B:** Diagram of precaudal vertebra from *M. californicus*, in lateral view, dissected from its neighbors at the intervertebral joints. Note the partial interdorsals and intervertebrals (iv) and the neural canal (nc) formed by the interdorsals and neural arches. Lateral processes (lp) and intervertebrals were removed for mechanical testing. **C:** Same as (B) but anterior view. **D:** Compression of a single vertebra, which includes the centrum, neural arch, and two half interdorsals (indicative of the "vertebrae" treatment category). The vertebra was loaded axially by non-porous platens touching its anterior and posterior surfaces. The compressive load was delivered via the actuator at a constant strain rate of  $2 \text{ mm s}^{-1}$  until the vertebra failed. With neural arch and half interdorsals removed, the sample would be indicative of the "centra" treatment category (see Fig. 4).

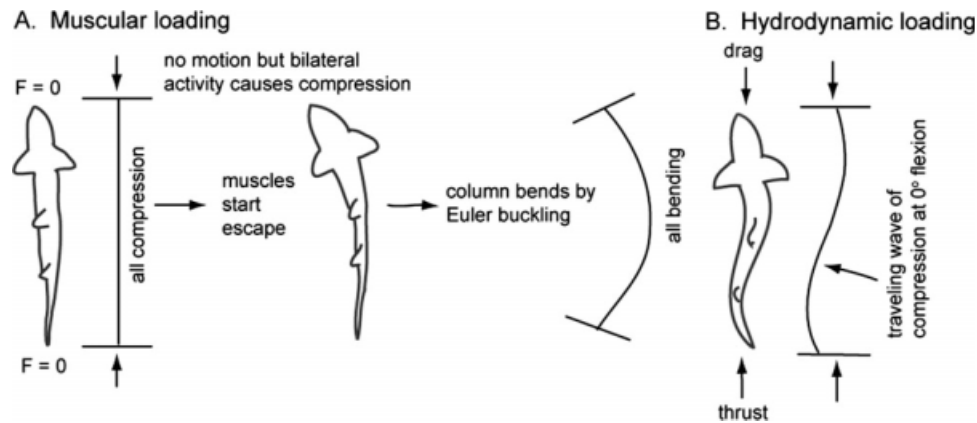


Fig. 2. Hypothetical model of the vertebral column loaded in compression *in vivo*. **A:** Muscular loading occurs during all forms of locomotion, but is likely maximized during the initiation of a fast-start startle response. Bilateral muscle activity, recorded in some teleost species (see text), would compress the body and the vertebral column prior to Euler buckling and the beginning of bending. **B:** Hydrodynamic loading occurs during all forms of locomotion but is likely maximized during fast cruising, when drag acting on the body is balanced by thrust at the tail, and the two forces compress and bend the body and the column.

occur, would be particularly problematic in cartilaginous skeletons because they lack blood vessels and cannot heal (Ashhurst, 2004).

## MATERIALS AND METHODS

### Anatomy and Species

Dissecting a vertebral column at the intervertebral joints creates segments consisting of a centrum, neural arch, and two partial and transected interdorsal cartilages (Fig. 1B). The neural arch, interdorsal cartilages, and dorsal margin of the centrum together form a hollow tube, the continuous neural canal (Fig. 1C). Medially, the centrum has a mineralized double-cone surrounded by mineralized adornments (see Fig. 3) that vary by species (Ridewood, 1921; Dean and Summers, 2006). The arch cartilages surmounting the centra of vertebrae found in the trunk region of the body are composed of tessellated cartilage, a core of unmineralized hyaline cartilage surrounded by a shell of mineralized blocks called tesserae (Ørving, 1951; Applegate, 1967; Moss, 1977; Kemp and Westrin, 1979; Dean and Summers, 2006).

Gray smooth-hound sharks, *Mustelus californicus* Gill 1864 (Carcharhiniformes: Triakidae), are found off the coast of southern California, and are small (total length ~110 cm), rapidly growing, and relatively short-lived (~10 years) sharks (Yudin and Cailliet, 1990; Compagno, 2003). The sharks were caught as by-catch in gill nets set overnight near shore as part of the Hubbs Sea World Research Institute Sea Bass Monitoring Program funded by the Ocean Resources Enhancement and Hatchery Program in southern California. *M. californicus* still alive in the nets were released; three sharks unintentionally killed as by-catch were available for this study. The carcasses were immediately brought back to the lab where vertebral columns were removed and frozen. Although the effects of freezing elasmobranch vertebral columns have not been studied, the effects on human vertebral columns have, and freezing does not alter their mechanical properties (Panjabi et al., 1985). Furthermore, freezing did not alter the mechanical properties of bovine articular cartilage (Keifer et al., 2005). Based on these results from mammalian vertebral columns and cartilage, we thus assume the same to hold true for the mineralized cartilage making up the vertebral columns of sharks. We studied multiple vertebrae from three subadult *M. californicus* of similar lengths: two 55 cm (total length, TL) females and one 54 cm (TL) male. We note

that *M. californicus* is a rapidly growing shark; males mature at 1–2 years, females at 2–3 years, and differential growth rates between sexes may influence mineral deposition (Yudin and

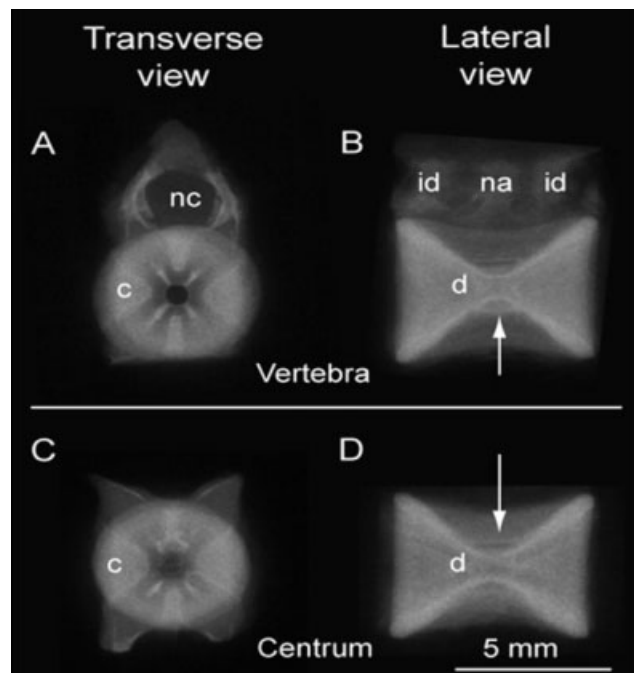


Fig. 3. Treatment categories for compression experiments (radiographs). **A, B:** The ‘vertebrae’ condition, with lateral processes removed but neural arch and interdorsals intact. Intensity of white indicates relative amount of mineralization. The double cone structure (d) and neural arch elements (na) are indicated, with the arrow denoting the apex of the mineralized double cone structure. **C, D:** The ‘centra’ condition, with all arches and processes removed. Because of the destructive nature of the testing, it was impossible to test a single vertebra both conditions. Note that in lateral view the double cone is the brightest, indicating a high level of total mineralization, when projected in 2D, compared with other structures.

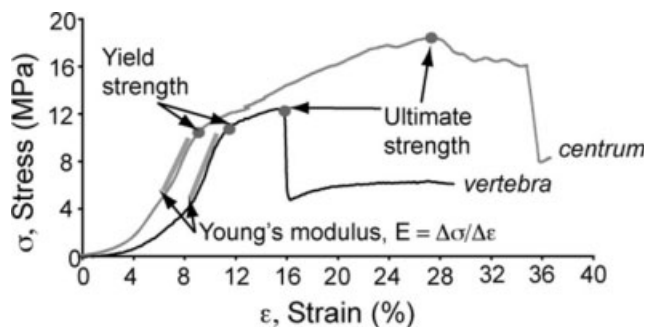


Fig. 4. Compression tests on a vertebra and centrum, example showing mechanical properties derived from the stress-strain curve. Yield strength is measured as the inflection point of the curve, marking where the transition occurs from elastic to plastic behavior. Ultimate strength is the maximum stress prior to failure. Young's modulus of elasticity is the slope of stress and strain in the linear elastic region. Note that centrum has higher stress values than the vertebra because it is calculated to have less total area to distribute the applied compressive force.

Cailliet, 1990) and hence compressive properties (Porter et al., 2007).

## Mechanical Testing

We tested individual vertebrae in compression. Although we recognize that vertebrae are compressed and bend during swimming (see Fig. 2), we isolate the compressive behavior for three reasons. First, from a theoretical engineering framework, compression and bending are additive, and thus can be measured independently (Den Hartog, 1956). Second, vertebrae, by virtue of their short axial length, have very small bending moments and thus, even in a bending body, are likely to be subjected primarily to compression. Third, from a practical point of view, we have been unable to grip and bend the short individual vertebra. We tested precaudal vertebrae from the region of the column in register with the first dorsal fin. We chose this area because the precaudal region in leopard sharks, *Triakis semifasciata*, undergoes less bending during swimming than the caudal region (Donley and Shadwick, 2003).

We thawed frozen vertebral columns by placing them in room temperature elasmobranch Ringers solution (Forster et al., 1972). Vertebrae were stored in solution in room temperature Ringer for no more than 2 h before mechanical testing (Porter et al., 2006). Twenty vertebrae from each animal were randomly assorted into our two treatment categories. Ten vertebrae from each animal had intact arch cartilages; we call this treatment condition "vertebrae" (Fig. 3A,B). The arch cartilages were removed via dissection from the other 10 vertebrae, leaving only the centra; we call this treatment condition "centra" (Fig. 3C,D). Arches were removed using a scalpel and care was taken to not cut into the mineralized centra (Porter et al., 2006, 2007). A small amount of nonload-bearing neural arch cartilage remained in each centrum where the arch inserts.

Each vertebra or centrum was tested in unconfin ed uniaxial compression to failure, at a constant strain rate of  $2 \text{ mm s}^{-1}$ , between two nonporous platens on an MTS MiniBionix 858 (Eden Prairie, MN) with a 5-kg load cell. This strain rate was chosen because it is used commonly in studies of articular cartilage (Li et al., 2003), though evidence from our previous compression tests on other shark vertebrae suggests that the mechanical properties measured here are independent of strain rate (Porter et al., 2007). The entire vertebra or centrum was compressed in the anterior-to-posterior direction, the orienta-

tion that mimics pure compressive load transfer from adjacent vertebrae *in vivo*.

Force, ( $F(N)$ )-displacement, ( $x \text{ (mm)}$ ), curves were obtained in real time at sampling rates of 1,000 Hz for each test and converted to stress-strain curves. Material properties were calculated using a custom script in Matlab version 7.0 R.12 (Mathworks, Natick, MA). This script converted force and displacement data into values of stress and strain and generated stress-strain curves for each sample. Engineering compressive stress was measured as  $F$  per initial cross-sectional area,  $A \text{ (m}^2\text{)}$  ( $\sigma = F/A$ ). Engineering compressive strain,  $\epsilon$ , measures the relative change in length of the vertebra under compression [ $\epsilon = (l_{\text{final}} - l_{\text{original}})/l_{\text{original}}$ ], where  $l_{\text{final}}$  is the length (mm) of the vertebra at the end of the compression test and  $l_{\text{original}}$  is the length (mm) before compression. Please note that  $\sigma$  and  $\epsilon$  use fixed cross-sectional area,  $A$ , and original length,  $l_{\text{original}}$ , as reference quantities. The  $A$  values were obtained using the projected 2D anterior surface of vertebrae and centra measured before testing; digital images were analyzed in ImageJ software (NIH). We recognize that instead of projected area, we might have used either the contact area of the rim and neural arch (Porter et al., 2006, 2007) or the total 3D surface area of the biconic intervertebral capsule and neural arch. However, as no measurements have ever been made of the stress transfer mechanism across elasmobranch intervertebral joints, we chose the intermediate projected  $A$  as our estimate. In sum, the calculation of  $\sigma$  and  $\epsilon$  involve assumptions that simplify the true nature of the vertebra, turning a complex structure into an idealized uniform shape with homogenous tissue properties. Thus caution should be used when comparing these values, and metrics obtained from them (see later), to those obtained in other structures and materials.

Maximum force at failure,  $F^*$ , was measured as the peak force during a trial. Yield strength,  $\sigma_y$  (Pa), is the elastic limit on a  $\sigma - \epsilon$  curve, and was operationally defined as the inflection point, which we selected manually as the point on the line at which the sign of the curvature changes (see Fig. 4). Yield strain,  $\epsilon_y$  (%), was determined at the corresponding  $\sigma_y$ . Apparent Young's modulus,  $E$  (Pa), an estimate of the material stiffness of the structure, was calculated as the slope of the linear region of the  $\sigma - \epsilon$  curve (Fig. 4; Wainwright et al., 1976). Ultimate strength,  $\sigma^*$  (Pa), was the maximum  $\sigma$  that a material can withstand before failing (see Fig. 4). Each of these properties was determined for each  $\sigma - \epsilon$  curve. For compressive  $\sigma$  and  $\epsilon$ , we use the positive sign convention sometimes used for the display of compression-only tests on bone (Currey, 2002).

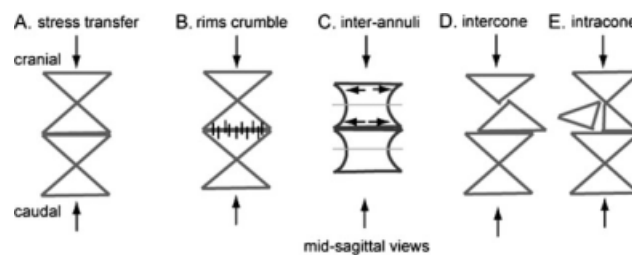


Fig. 5. Compressive loading and possible fracture patterns. Diagrams, mid-sagittal view, of a motion segments, vertebra-joint-vertebra, with vertebrae represented by the double cone that is the primary mineralized structure of the centrum (see Fig. 3), loaded axially (vertical arrows). **A:** During compression, stress transfers via the intervertebral ligament from rim to rim of the adjacent cone. **B:** Rims crumble: failure occurs at the rims of the double cone, absorbing the work of fracture. **C:** Inter-annuli: failure occurs between the growth rings, or annuli, within the cones (noted by Porter et al., 2006). **D:** Intercone: failure occurs when the apices connecting cones dislocates. **E:** Intracone: failure occurs when one cone cracks radially.

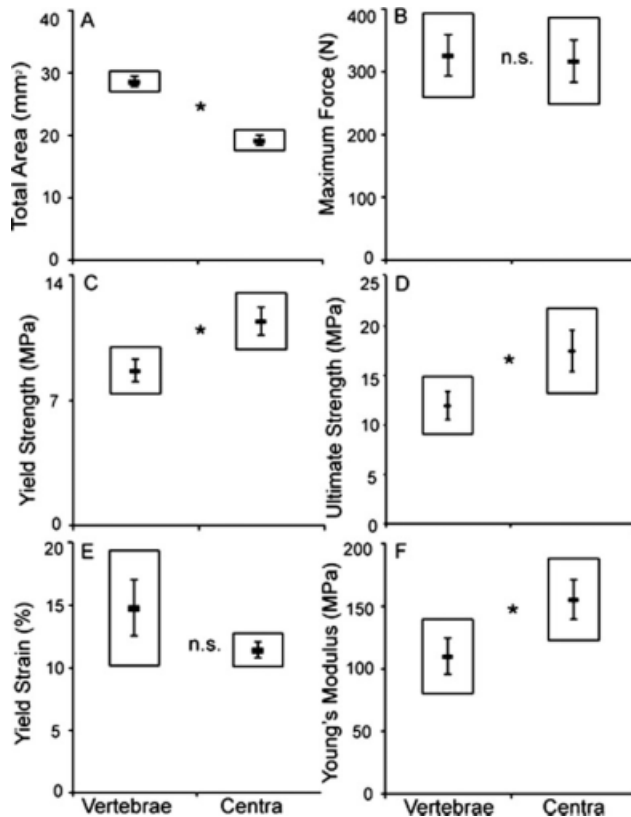


Fig. 6. Mechanical properties of the vertebrae and centra, loaded in compression until failure, of *M. californicus*. **A:** Total cross-sectional area was greater in vertebrae ( $P < 0.001$ ). **B:** Maximum force to failure was statistically indistinguishable in the vertebrae and the centra. **C:** Ultimate strength was greater in centra ( $P = 0.0002$ ). **D:** Yield strength was greater in centra ( $P = 0.0073$ ). **E:** Yield strain was statistically indistinguishable in both structures ( $P = 0.21$ ). **F:** Young's modulus was greater in centra ( $P = 0.0049$ ). Data are shown as box-and-whisker plots where the narrow horizontal rectangle represents the mean for each group, the boxes are 95% confidence intervals around that mean, and the whiskers are  $\pm$  one s.e.m. A total of 60 vertebrae ( $n = 30$ ) and centra ( $n = 30$ ) from three sharks were tested. Statistics were performed on data transformed to achieve normal distribution (see Methods for details). Asterisks indicate significant differences ( $P < 0.05$ ) between treatment categories. Please note that plots show nontransformed values, even though the statistical analysis was conducted on the transformed data. See Table 1 for statistical results.

### Statistical Analysis

We used a repeated-measures MANOVA to account for the within-individual sampling design (JMP 5.0.1a, SAS Institute; Zar, 1999). This design tests for effects of treatment, individual shark, and the interaction between treatment and individual. The factor "treatment" consisted of two categories, either the "vertebrae" or "centra" condition described in the previous section.  $A$  was normally distributed as determined using a Shapiro Wilk  $W$  test.  $E$ ,  $\sigma_y$ , and  $\varepsilon_y$  were all normally distributed, as determined by the Kolmogorov-Smirnov test, after log transformation.  $F^*$  and  $\sigma^*$ , as determined by the Kolmogorov-Smirnov test, were normally distributed following inverse transformation. All variables passed the Mauchly Criterion for sphericity, except  $E$  and  $\varepsilon_y$ . To account for this, results for  $E$  and  $\varepsilon_y$  are

shown using the univariate Huynh-Feldt Epsilon test; all other variables were tested using univariate  $F$ -tests.

Anterior and lateral view contact radiographs of vertebrae and centra were taken in a cabinet radiograph machine with Kodak Bio-Max film before and after mechanical testing to determine the fracture pattern of the mineralized cartilage during compression to failure. Fracture patterns were scored based on the nature of damage to the vertebra or centra (see Fig. 5). Fracture data were analyzed using contingency tables (Chi square) in Excel to determine if the fracture patterns differed from each other by category (vertebra v. centra) and differed from an even distribution (Zar, 1999).

### RESULTS

As expected, vertebrae had a significantly larger total area,  $A$ , than centra (Fig. 6A). Maximum force,  $F^*$ , did not vary between the vertebrae and the centra (Fig. 6B), even though  $A$  for the vertebrae is greater than that for the centra. Compared with vertebrae, the centra had larger ultimate strength,  $\sigma^*$ , yield strength,  $\sigma_y$ , and Young's modulus,  $E$  (Fig. 6C–E). A statistically significant treatment effect was detected for  $A$ ,  $\sigma^*$ ,  $\sigma_y$ , and  $E$  (Table 1). Significant individual effects were detected for all variables except yield strain,  $\varepsilon_y$ . The interaction between treatment and individual was not significant in any case.

In all mechanical tests, vertebrae failed at the centrum but not at the arch, as determined by visual and radiographic inspection (Fig. 7A–C). For fracture patterns occurring in vertebrae, the type of fracture did not occur evenly ( $\chi^2 = 7.867$ ,  $P = 0.049$ ); inter- and intracone failures occurred more often than compound and other fracture types (Fig. 7C). For fracture patterns occurring in centra, the type of fracture occurred evenly across types ( $\chi^2 = 4.400$ ,  $P = 0.221$ ), even though no significant difference was detected between the distribution of failure patterns in vertebrae and centra ( $\chi^2 = 0.876$ ;  $P = 0.831$ ). Because no difference was detected between treatments, we pooled the groups and found that the fracture pattern of vertebrae and centra, combined, differed from an even distribution ( $\chi^2 = 88.43$ ;  $P = 0.00785$ ); inter- and intracone fractures occurred more often than compound and other types. Centra had two distinct fracture patterns primarily taking place within the double cone structure (see Fig. 7).

### DISCUSSION

We measured the compressive properties of vertebrae and centra. The two structures, differing by the presence of a neural arch, sustain statistically indistinguishable maximum compressive forces (Fig. 6B). Under *in vitro* testing conditions, where the arch and centra are simultaneously in contact with the load-imposing platens (see Fig. 1), we conclude that the arch does not bear appreciable loads because vertebrae are less stiff than centra (Fig. 6F). Independent evidence for this conclusion

TABLE 1. Structural and mechanical properties of vertebrae and centra as tested by repeated measures ANOVA

Response variable	Treatment			Individual			Interaction		
	<i>F</i> stat	<i>P</i> value	DF	<i>F</i> stat	<i>P</i> value	DF	<i>F</i> stat	<i>P</i> value	DF
Total area (mm <sup>2</sup> )	69.37	<0.0001	1,18	2.29	0.1313	2,17	0.66	0.530	2,17
Maximum force (N)	0.35	0.5603	1,17	31.78	<0.0001	2,16	0.62	0.552	2,16
Ultimate strength (MPa)	21.9	0.0002	1,17	25.01	<0.0001	2,16	1.67	0.220	2,16
Yield strength (MPa)	9.14	0.0073	1,18	18.96	<0.0001	2,17	0.49	0.6212	2,17
Young's modulus (MPa)	10.46	0.0049	1,17	6.61	0.008	2,16	0.02	0.979	2,16
Yield strain (%)	0.21	0.6500	1,17	140.0	<0.0001	1,18	0.50	0.503	1,18

Total length was normally distributed. Young's modulus, yield strain, and yield strength were normally distributed after log transformation. Maximum force and ultimate strength were normally distributed after inverse transformation. As yield strain failed the Mauchly criterion for sphericity, we used the univariate Huynh-Feldt Epsilon test on that variable.

comes from the fact that vertebrae fail in compression at the centra, and not at the arches (see Fig. 7). If the *in vitro* testing condition approximates the loading condition *in vivo*, then we predict that during swimming (see Fig. 2), too, compressive loads acting on the vertebral column are borne by the centra. These results support the hypothesis that the evolution of centra, which occurred after the origin of neural arch structures, might have been an adaptation for enhanced swimming performance made possible by an increased capacity for compressive load-bearing by the body axis. Determining the magnitude of this increase will, ultimately, require direct assessment of the arch properties. However, if axial stiffness is correlated with swimming speed, as indicated by data from robot performance (Long et al., 2006), then such measurements might provide a quantitative assessment of the effects of centra on swimming performance.

These results leave unresolved several additional questions that we explore further in the following sections: (1) What mechanical function, if any, does the neural-interdorsal arch have when the vertebra is compressed? (2) Are vertebrae ever in danger of compressive failure in life? (3) How do the compressive properties of shark vertebrae, composed of mineralized cartilage, compare with those of bone?

### Mechanical Function of the Arches in Compression?

Strictly speaking, we do not know the mechanical behavior of the arches by themselves. As noted in the Introduction, we were unable to conduct experiments on isolated arches. Hence, we infer arch function from the comparison of vertebrae, with arches, to centra, lacking arches. We assume that differences between the two conditions are additive, and would expect that if arches had a Young's modulus,  $E$ , equal to or greater than that of the centra then the  $E$  of the vertebrae should be equal to or greater than that of the centra. However, we acknowledge that evidence is less strong than that for comparisons of maximum force ( $F^*$ )

data because of the simplifying assumptions involved in calculating  $E$ , mentioned in the Methods.

Although they may not bear substantial compressive loads compared with the centra, arches

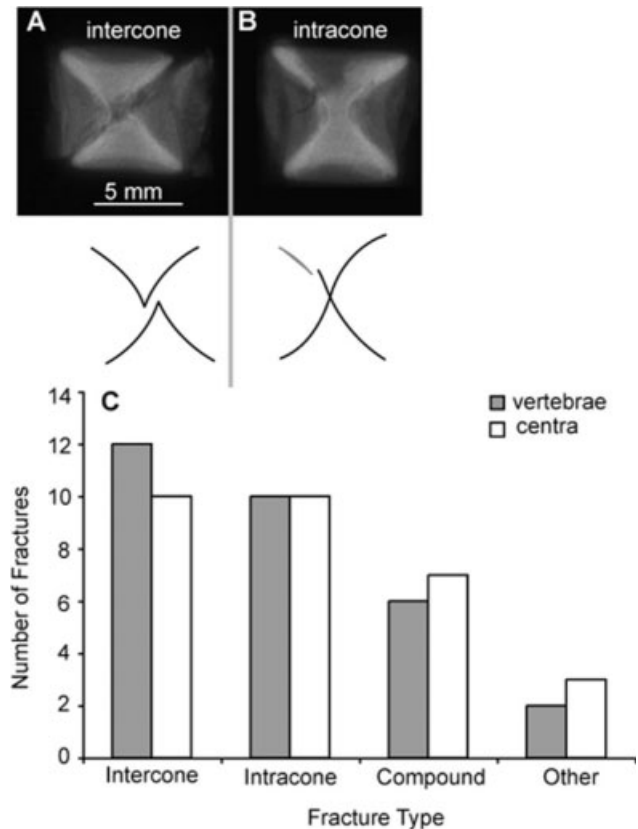


Fig. 7. Failure patterns of vertebrae and centra under compressive loads. A. Intercone shearing, example of failure of the double cone at the apices, shown in X-ray, lateral view. This was the most common fracture pattern in vertebrae. B. Intracone fracture, example of failure within cone by radial cracking or annuli separation, shown in X-ray, lateral view. C. The patterns of failure. Distribution of fracture patterns of the vertebrae ( $\chi^2 = 7.867$ ;  $P = 0.049$ ) but not the centra ( $\chi^2 = 4.40$ ;  $P = 0.221$ ) differed significantly from an even distribution. Patterns for vertebrae and centra did not differ significantly from each other.

may alter the stress distribution in the vertebrae as the centra are failing. Fractures in vertebrae, which always take place in the centra and never in the arches, occur in a pattern that deviates from an expected even distribution; in contrast, fracture patterns in centra do not deviate from an even distribution (Fig. 7C). We propose that as a vertebra fails, the centrum's  $E$  rapidly drops below that of the arch, momentarily causing the arch to bear more stress. This shift may account for the differences in mode of failure between centra and vertebrae. If vertebral fractures by compression occur in a shark, then stress-bearing by the arches may delay or forestall compression of the spinal cord housed medial to the arches. This interpretation is weakened, however, by the fact that the fracture patterns of vertebrae and centra, when compared with each other, as opposed to a pattern of even distribution, do not differ statistically.

### Are Vertebrae Ever in Danger of Compressive Failure in Life?

To predict if vertebrae may fail in compression *in vivo*, we need to estimate what the maximal compressive loads might be and when they might occur. Of course, these interpretations are speculative and conclusions should be treated cautiously because in life centra are loaded as part of an entire column rather than as single elements.

Shark vertebral columns may experience pure compression at specific moments and locations during the initiation of a fast start or when drag and thrust are equal and opposite during steady swimming (see Fig. 2). At the onset of a fast start, bilateral muscle activity has been shown in several species of fishes (Westneat et al., 1998; Hale et al., 2002; Tytell and Lauder, 2002). Thus, when muscles contract bilaterally, the vertebral column may be placed instantaneously in pure compression, which, *via* Euler buckling, may initiate bending of the body (Czuwala et al., 1999). If this were the case, how much muscle force,  $F_m$ , might be acting on the vertebrae and what are the safety factors for shark vertebrae during a fast start?

To generate a crude first approximation of the  $F_m$ , we first assume that a shark is a uniform right circular cylinder made entirely of white muscle with a density of  $1,060 \text{ kg m}^{-3}$ . Using this body density,  $\rho_b$ , and body mass,  $m_b$ , from *Mustelus canis* (570 g for a 55 cm long animal; van der Elst, 1981), we can estimate shark body volume,  $V_b$ , and then body cross-sectional area,  $A_b$ , as follows:

$$V = \frac{m_b}{\rho_b} \text{ and } A_b = \frac{V_b}{l_b}$$

where  $l_b$  is the length of the body. We use our estimate of  $A_b$  to calculate the  $F_m$ ; we divide muscle

stress,  $241 \text{ mN mm}^{-2}$  for isometric contraction in the white muscle of *Scyliorhinus canicula*, (Curtin and Woledge, 1988), by  $A_b$ . This formulation yields an estimation of a maximum  $F_m$  of 235 N.

In addition to the possible compressive loads imposed by  $F_m$ , the vertebral column may also experience compression from hydrodynamic loading during steady swimming, when drag,  $D$  (N), and thrust,  $T$  (N), are acting in opposition, per Newton's third law, primarily on the anterior and posterior parts of the body, respectively (see Fig. 2B).  $D$  is defined as follows:

$$D = \frac{1}{2} C_D \rho S U^2,$$

where  $C_D$  is the drag coefficient,  $\rho$  is density of seawater,  $S$  is the wetted surface area of the body, and  $U$  is the swimming speed. If we again assume, as a crude approximation, that the shark is a right circular cylinder, we calculate  $S$  as the product of  $l_b$  and the circumference of the cylinder. Using a  $C_D$ , 0.04, for a streamlined body and  $\rho$  of seawater at  $20^\circ\text{C}$  (Vogel, 1994), we estimate that the  $D$  acting on a shark at any given  $U$  ranges from 3.8 N at  $1 \text{ m s}^{-1}$  to 15.2 N at  $2 \text{ m s}^{-1}$ . These values of  $D$  are small compared with those of  $F_m$ ; taken together, they sum to maximum compressive loads of 250 N, still below the maximum  $F^*$  values measured for vertebrae and centra (see Fig. 6).

Using the value of 250 N for combined muscular and hydrodynamic compressive loads, and a mean  $F^*$  for vertebrae of 304 N (Fig. 6B), these values yield a safety factor of 1.2. If we follow the advice of Biewener (1993) and use a force associated with yield strength,  $\sigma_y$ , rather than ultimate strength,  $\sigma^*$  (see Fig. 6C,D for an approximate ratio of 9 to 12 MPa, respectively) we would lower  $F^*$  to 228 N, yielding a minimum safety factor of 0.9. One interpretation of this result is that the vertebral column will fail if and when the maximum compressive forces are generated. With a minimum safety factor near one, we would expect to see many more fractures than the few indicated by indirect evidence in living sharks (Hoenig and Walsh, 1983; Officer et al., 1995; Porter et al., 2006). On the other hand, it is more likely that we have overestimated  $F_m$ . If instead of assuming bilateral activity, we assume unilateral activity, the  $F_m$  would decrease by half to 117.5 N. Adding the hydrodynamic load of 15 N for a total load of 132.5 N, the safety factor becomes 2.3. Estimates of safety factors would continue to rise if we made our model more realistic by including noninstantaneous muscle activation, muscle fiber angles, and red muscle. In addition, safety factors might be increased in life by the serial arrangement of vertebrae in a column, an arrangement that may predispose axial compressive loads to cause Euler buckling of the

column before those same loads can reach levels that would cause vertebral failure. If these higher safety factors are more accurate, then vertebral fractures, when and if they occur, may be caused by pressure from predatory or mating bites or by developmental abnormalities. Finally, please keep in mind when considering these arguments about safety factors that because the vertebral column fractures observed in sharks have not been verified as matching those observed in these *in vitro* mechanical tests, the actual *in vivo* loading regime has not been established.

### How do the Compressive Properties of Shark Vertebrae Compare With Those of Bone?

The compressive properties of the mineralized, cartilaginous vertebrae of sharks show much greater strength for a given  $E$  than that of the cancellous bone of *Bos taurus* (see Fig. 8). To generate this comparison, we combined data from this study with that from our previous work on the vertebrae of the following shark species: *Isurus oxyrinchus*, *Sphyrna zygaena*, *Carcharhinus falciformis*, *Carcharhinus plumbeus*, *Centrophorus granulosus*, *Torpedo californica*, a *Centrophorus* sp., and *Mustelus californicus* (Porter et al., 2006, 2007). Data on the cancellous bone of cattle are from compression tests conducted by Currey (2002) and Hodgkinson and Currey (1992).

Recalling that  $E$  is material stiffness, we can compare strength-to-stiffness ratios. For bovine cancellous bone, the strength-to-stiffness ratio is 0.01, a value that appears to be typical for mammalian bone of different types, including compact bone, and bone from different mammalian species (Hodgkinson and Currey, 1990, 1992; Curry, 1999). For the vertebral cartilage of sharks, we estimate the strength-to-stiffness ratio to be 0.05, a fivefold increase relative to mammalian bone. This dramatic difference, if consistent across elasmobranch (sharks, skates, and rays) and mammalian species, may suggest an evolutionary trade-off in the mechanical design of skeletons: cartilaginous skeletons may be selected for high ultimate strength, at the cost of reduced Young's modulus, and bony skeletons may be selected for high Young's modulus, at the cost of reduced ultimate strength.

It is important to note that vertebrae are the only known structures in elasmobranch skeletons that are composed of three types of mineralized cartilage: areolar, prismatic, and globular (Ørvig, 1951; Kemp and Westrin, 1979; Dean and Summers, 2006). Other skeletal structures possess only prismatic and globular calcification (Ørvig, 1951; Applegate, 1967; Moss, 1977; Kemp and Westrin, 1979; Dean and Summers, 2006) that form tiny mineralized blocks covering a hyaline core, together forming a cartilage type recently

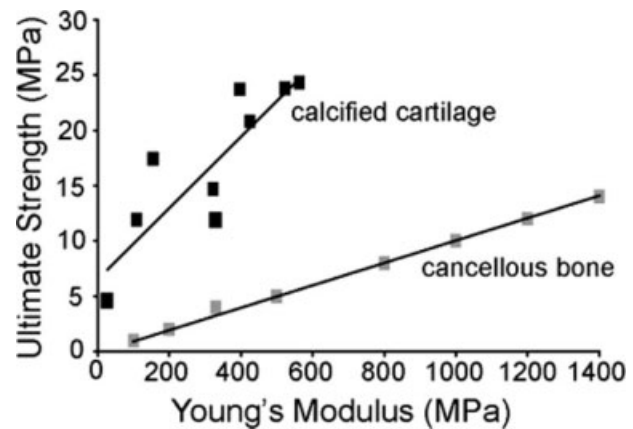


Fig. 8. The mineralized vertebrae of sharks are stronger in compression, at a given Young's modulus, than the cancellous bone of mammals (*Bos taurus*). Thus, the vertebral cartilage strength-to-stiffness ratio in elasmobranchs (black squares) is approximately five times larger than that of cancellous bone (gray squares). Elasmobranch data points include data from the present study (one point) and also values presented in previous work on mineralized cartilaginous vertebrae from *Isurus oxyrinchus*, *Sphyrna zygaena*, *Carcharhinus falciformis*, *Carcharhinus plumbeus*, *Centrophorus granulosus*, *Torpedo californica*, and a *Centrophorus* sp. (Porter et al., 2006, 2007). The final elasmobranch datum comes from a separate sample of *Mustelus californicus* (Porter et al., 2007), which were included here because they are from individuals of a larger size than those tested in this study.

termed "tessellated" (Dean and Summer, 2006). Little is known about the mechanical properties of tessellated skeletal elements (Summers et al., 1998; Summers, 2000; Dean and Summers, 2006; Porter et al., 2006, 2007). Even so, it appears that within elasmobranchs, the mechanical properties of vertebrae, as controlled by kinds and degrees of mineralization, have been targeted, separate from other skeletal elements, by selection for enhanced strength.

In conclusion, centra are the primary load-bearing structures of the vertebrae in compression. The arch, while not adding significantly to compressive load resistance, may act to alter stress distribution, as suggested by differences in fracture patterns in centra and vertebrae treatments. These results support the hypothesis that the evolution of centra, which occurred after the origin of neural arch structures, might have been an adaptation for increased axial stiffness (Laerm 1976; Wainwright et al., 1978), that could, in turn, have increased swimming speed (Clark, 1964; Long et al., 2006). However, in axially undulating vertebrates, vertebral columns are loaded in both compression and bending during swimming. Under those more realistic conditions of superimposed loads, it is possible that arches have a different function, perhaps, by virtue of spanning the intervertebral joint (see Fig. 1), preventing or reducing shearing and dislocation of the joints in concert with the intervertebral ligaments.

## ACKNOWLEDGMENTS

Members of Adam Summers' and Matt McHenry's biomechanics labs at the University of California, Irvine, provided helpful comments on earlier drafts of the manuscript. On later versions, the Vassar College Fish Fellows (generation 4) provided substantial comments. Two anonymous reviewers provided careful and critical comments. The mechanical experiments took place in the lab of Thomas Koob; he and his lab members graciously provided us with time and assistance. Vertebral columns used in this experiment were provided by the Hubbs Sea World Research Institute Sea Bass Monitoring Program, which was funded by Ocean Resources Enhancement and Hatchery Program. L. Whitenack, C.J. Tibbits and T. Tibbits provided assistance while conducting these experiments.

## LITERATURE CITED

- Applegate SP. 1967. A Survey of Shark Hard Parts. Maryland: Johns Hopkins Press.
- Arratia G, Schultze H-P, Casciotta J. 2001. Vertebral column and associated elements in dipnoans and comparison with other fishes: Development and homology. *J Morphol* 250:101–172.
- Ashhurst DE. 2004. The cartilaginous skeleton of an elasmobranch fish does not heal. *Matrix Biol* 23:15–22.
- Biewener AA. 1993. Safety factors in bone strength. *Calcif Tissue Int* 53(suppl 1):S68–S74.
- Clark RB. 1964. Dynamics in Metazoan Evolution: The Origin of the Coelom and Segments. London: Oxford University Press.
- Compagno LJV. 2003. Sharks of the Order Carcharhiniformes. Caldwell, NJ: Blackburn Press.
- Currey JD. 1999. The design of mineralised hard tissues for their mechanical functions. *J Exp Biol* 202:3285–3294.
- Currey JD. 2002. Bones. Princeton: Princeton University Press.
- Curtin NA, Woledge RC. 1988. Power output and force-velocity relationship of live fibers from white myotomal muscle of the dogfish, *Scyliorhinus canicula*. *J Exp Biol* 140:187–197.
- Czuwala PJ, Blanchette C, Varga S, Root RG, Long JH, Jr. 1999. A mechanical model for the rapid body flexures of fast-starting fish. In: Proceedings of the 11th International Symposium on Unmanned Untethered Submersible Technology (UUST). Autonomous Undersea Systems Institute, Lee, NH. pp 415–426.
- Den Hartog JP. 1956. Mechanical Vibrations, 4th ed. New York: McGraw-Hill Book Company.
- Dean MN, Summers AP. 2006. Mineralized cartilage in the skeleton of chondrichthyan fishes. *Zoology* 190:164–168.
- Donley JM, Shadwick RE. 2003. Steady swimming muscle dynamics in the leopard shark *Triakis semifasciata*. *J Exp Biol* 206:1117–1126.
- Donley JM, Sepulveda CA, Konstantinidis P, Gemballa S, Shadwick RE. 2004. Convergent evolution in mechanical design of lamnid sharks and tunas. *Nature* 429:61–65.
- Doorly N, Irving K, McArthur G, Combie K, Engel V, Sakhtah H, Stickles E, Rosenblum H, Gutierrez A, Root R, Liew C-W, Long JH Jr. 2009. Biomimetic evolutionary analysis: Robotically-simulated vertebrates in a predator-prey ecology. Proceedings of the 2009 IEEE Symposium on Artificial Life, USA, 147–154.
- Forster RP, Goldstein L, Rosen JK. 1972. Intrarenal control of urea reabsorption by renal tubules of the marine elasmobranch, *Squalus acanthias*. *Comp Biochem Physiol A* 42:3–12.
- Gardiner BG. 1983. Gnathostome vertebrae and the classification of the amphibia. *Zool J Linn Soc* 79:1–59.
- Gemballa S, Konstantinidis P, Donley JM, Sepulveda C, Shadwick RE. 2006. Evolution of high-performance swimming in sharks: Transformations of the musculotendinous system from subcarangiform to thunniform swimmers. *J Morphol* 267:477–493.
- Goodrich ES. 1930. Studies on the Structure and Development of Vertebrates. USA: The University of Chicago Press.
- Hale ME, Long JH Jr, McHenry MJ, Westneat MW. 2002. Evolution of behavior and neural control of the fast-start escape response. *Evolution* 56:993–1007.
- Heupel MR, Simpfendorfer CA, Bennett MB. 1999. Skeletal deformities in elasmobranchs from Australian waters. *J Fish Biol* 54:1111–1115.
- Hodgkinson R, Currey JD. 1990. Effects of structural variation on the Young's modulus of non-human cancellous bone. *Eng Med* 204:43–52.
- Hodgkinson R, Currey JD. 1992. Young's modulus, density and material properties in cancellous bone over a large density range. *J Mater Sci Mater Med* 3:377–381.
- Hoening JM, Walsh AH. 1983. Skeletal lesions and deformities in large sharks. *J Wildl Dis* 19:27–33.
- Kiefer GN, Sundby K, McAllister D, Shrive NG, Frank CB, Schachar NS. 2005. The effect of cryopreservation on the biomechanical behavior of bovine articular cartilage. *J Orthop Res* 7:494–501.
- Kemp NE, Westrin SK. 1979. Ultrastructure of calcified cartilage in the endoskeletal tesserae of sharks. *J Morphol* 160:75–102.
- Koob TJ, Long JH. 2000. The vertebrate body axis: Evolution and mechanical function. *Am Zool* 40:1–18.
- Laerm J. 1976. The development, function, and design of amphicoelous vertebrae in teleost fishes. *Zool J Linn Soc* 58:237–254.
- Laerm J. 1979. On the origin of Rhipidistian vertebrae. *J Paleontol* 53:175–186.
- Li LP, Buschman MD, Shirazi-Adl A. 2003. Strain-rate dependent stiffness of articular cartilage in unconfined compression. *J Biomech Eng* 125:161–186.
- Long JH. 1992. Stiffness and damping forces in the intervertebral joints of blue marlin (*Makaira nigricans*). *J Exp Biol* 162:131–155.
- Long JH Jr, Koob-Emunds M, Koob TJ. 2004. The mechanical consequences of vertebral centra. *Bull Mt West Isl Biol Lab* 43:99–101.
- Long JH Jr, Koob TJ, Irving K, Combie K, Engel V, Livingston N, Lammert A, Schumacher J. 2006. Biomimetic evolutionary analysis: Testing the adaptive value of vertebrate tail stiffness in autonomous swimming robots. *J Exp Biol* 209:4732–4746.
- Moss ML. 1977. Skeletal tissues in sharks. *Am Zool* 17:335–342.
- Officer RA, Clement JG, Rowler DK. 1995. Vertebral deformities in a school shark *Galeorhinus galeus*: Circumstantial evidence for endoskeletal resorption? *J Fish Biol* 46:85–98.
- Ørvig T. 1951. Histologic studies of placoderm and fossil elasmobranchs. I. The endoskeleton, with remark on the hard tissues of lower vertebrates in general. *Arch fur Zool* 2:312–454.
- Panjabi MM, Krag M, Summers D, Videman T. 1985. Biomechanical time-tolerance of fresh cadaveric human spine specimens. *J Orthop Res* 3:292–300.
- Porter ME, Beltrán JL, Koob TJ, Summers AP. 2006. Material properties and biochemical composition of mineralized vertebral cartilage in seven elasmobranch species (Chondrichthyes). *J Exp Biol* 209:2920–2928.
- Porter ME, Koob TJ, Summers AP. 2007. The contribution of mineral to the material properties of vertebral cartilage from the smooth-hound shark *Mustelus californicus*. *J Exp Biol* 210:3319–3327.
- Ridewood WG. 1921. On the calcification of the vertebral centra in sharks and rays. *Philos Trans R Soc Lond B Biol Sci* 210:311–407.

- Rogers RR, LaBarbera M. 1993. Contribution of internal bony trabeculae to the mechanical properties of the humerus of the pigeon (*Columba livia*). *J Zool* 230:433–441.
- Schaeffer B. 1967. Osteichthyan vertebrae. *J Linn Soc Lond Zool* 47:185–195.
- Summers AP. 2000. Stiffening the stingray skeleton—An investigation of durophagy in myliobatid stingrays (Chondrichthyes, Batoidea, Myliobatidae). *J Morphol* 243:113–126.
- Summers AP, Koob TJ, Brainerd EL. 1998. Stingray jaws strut their stuff. *Nature* 395:450–451.
- Tytell ED, Lauder GV. 2002. The C-start escape response of *Polypterus senegalus*: Bilateral muscle activity and variation during stage 1 and 2. *J Exp Biol* 205:2591–2603.
- van der Elst R. 1981 *A Guide to the Common Sea Fishes of Southern Africa*. Cape Town: C. Struik.
- Vogel S. 1994. *Life in Moving Fluids*. Princeton, NJ: Princeton University Press.
- Vogel S. 2003. *Comparative Biomechanics: Life's Physical World*. Princeton, NJ: Princeton University Press.
- Wainwright SA, Biggs WD, Currey JD, Gosline JM. 1976. *Mechanical Design in Organisms*. Princeton, NJ: Princeton University Press.
- Wainwright SA, Vosburgh F, Hebrank JH. 1978. Shark skin: Function in locomotion. *Science* 202:747–749.
- Westneat MW, Hale ME, McHenry MJ, Long JH Jr. 1998. Mechanics of the fast-start: Muscle function and the role of intermuscular pressure in the escape behavior of *Amia calva* and *Polypterus palmas*. *J Exp Biol* 201:3041–3055.
- Yudin KG, Cailliet GM. 1990. Age and growth of the Gray Smoothhound, *Mustelus californicus*, and the Brown Smoothhound, *M. henli*, Sharks from Central California. *Copeia* 1990:191–204.
- Zar JH. 1999. *Biostatistical Analysis*. New Jersey: Prentice Hall.